THE JOURNAL OF PHYSICAL CHEMISTRY C
A JOURNAL OF THE AMERICAN CHEMICAL SOCIETY

pubs.acs.org/JPCC Article

Role of Oxygen Vacancy Sites on the Temperature-Dependent Photoluminescence of SnO_2 Nanowires

Euiyoung Choi, Dongwook Lee,* Hyun-Joon Shin, Namdong Kim, L. De Los Santos Valladares, and Jiwon Seo*

Cite This: https://doi.org/10.1021/acs.jpcc.1c02937 Read Online

ACCESS | Metrics & More | Article Recommendations | Supporting Information

ABSTRACT: The role of oxygen vacancies in temperature-dependent photoluminescence of SnO_2 nanowires was investigated by X-ray absorption spectroscopy. Two types of oxygen vacancies are present in the nanowires: at out-of-plane sites and at in-plane sites; both play crucial roles in the temperature dependence of the photoluminescence. Oxygen vacancies at in-plane sites participate in photon emission at low temperature, whereas those at out-of-plane sites result in photoluminescence at room temperature. Accordingly, the luminescence color changes from orange (630 nm, 1.93 eV) to green (515 nm, 2.4 eV) at 100 K. The color change is accompanied with a notable change in the oxygen *K*-edge X-ray absorption spectra. The scanning transmission X-ray microscopy results indicate that more oxygen vacancies at in-plane sites are present in the surface region than in the bulk region, whereas more oxygen vacancies at out-of-plane sites are present in the bulk region than in the surface region. Overall, the results demonstrate that oxygen-vacancy-mediated fluorescence properties of SnO_2 nanowires are temperature-dependent; i.e., the photoluminescence mechanisms of the nanowires are mediated by oxygen vacancies at different sites, and the bicolor fluorescence originates from charge transfer between the states.

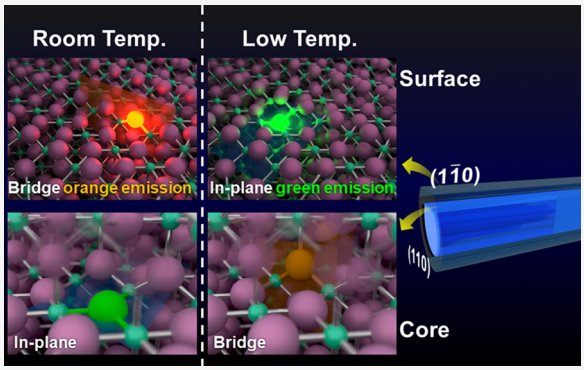

1. INTRODUCTION

Tin dioxide (SnO_2) is a typical example of Janus-like transparent conductors, which exhibit the contradictory properties of insulator-like transparency due to a wide bandgap (3.6 eV) and high metallic conductivity caused by massive structural nonstoichiometry and oxygen vacancies.[1−3] Oxygen vacancies in SnO_2 have a surprisingly low formation energy and donate electrons to the conduction band.[4] Thus, SnO_2 is electrically conductive and transparent in the visible range. The n-type wide bandgap and high conductivity of SnO_2 make it a promising candidate for applications in various devices, such as transparent electrodes, sensors, optoelectronics devices, and solar cells.[5−12] With increasing interest in the nanoregime, the synthesis of nanosize tin dioxides has become a focus of research. Nanostructured SnO_2, such as nanowires and nanobelts, has been well received because it can be applied in gas sensors owing to the large surface area and the presence of surface defects, which make it suitable for the adsorption of gas molecules. Defects in bulk-scale SnO_2 have not attracted attention because their contribution to the properties of bulk SnO_2 is negligible. However, they have attracted attention owing to their crucial effects on the electrical and optical properties of nanosize SnO_2 as the size decreases further into the nanometer regime.

Among the defects in SnO_2, oxygen vacancies in SnO_2 change the electrical, optical, and even catalytic properties of the material. When SnO_2 is used in transparent electrodes for displays, the oxygen vacancies cause instability originating from negative bias illumination stress.[13,14] Interfacial oxygen vacancies are the origin of hysteresis in perovskite solar cells.[15] Oxygen vacancies in SnO_2 are gas adsorption sites and control the sensing selectivity and the stability.[16−19] Thus, they affect the efficiency, device stability, and sensitivity. However, oxygen vacancies in oxides, including SnO_2, have not been thoroughly investigated. Although heat treatment such as annealing in an inert gas is well known to reduce oxygen vacancies in oxides, the distribution of vacancies in oxides is still unclear. Here, we report that two types of oxygen vacancies are present in SnO_2 nanowires and that they migrate with temperature, contributing to the photoluminescence (PL) by causing the colors to change with temperature.

Received: April 1, 2021
Revised: June 10, 2021

https://doi.org/10.1021/acs.jpcc.1c02937
J. Phys. Chem. C XXXX, XXX, XXX−XXX

2. METHODS

SnO_2 nanowires were grown on a z-cut quartz substrate with a thickness of 0.5 mm by chemical vapor deposition. First, a mixture of ethanol and PEG600 with a volume ratio of 5: 1 was prepared. $H_2C_2O_4$ (5 mmol) was then dissolved in 40 mL of the above mixture under continuous magnetic stirring until $H_2C_2O_4$ was dissolved completely. Subsequently, 5 mmol $SnCl_2{\cdot}2H_2O$ was added into the above solution followed by dropwise addition of 10 mL of deionized water. After continuous stirring for 30 min, the mixed solution was washed several times with ethanol and deionized water. The product was dried in a chamber furnace at 60 °C for 8 h and finally annealed in a muffle kiln at 600 °C for 2 h. The structural and morphological properties of SnO_2 nanowires were characterized by X-ray powder diffraction (XRD, Bruker D8 Avance Cu Kα), scanning electron microscopy (SEM, JSM-6700F), and Raman spectroscopy (Horiba Labram HR) using 325 nm/532 nm lasers. The PL spectra at different temperatures were acquired from 350 to 850 nm using a 325 nm He−Cd laser (Horiba Labram HR).

X-ray absorption spectroscopy and scanning transmission X-ray microscopy measurements were conducted at 10A Beamline in Pohang Accelerator Laboratory (PAL). The XAS spectra were collected in transmission mode.

3. RESULTS AND DISCUSSION

Figure 1(a,b) shows typical SEM images of SnO_2 nanowires prepared on a z-cut quartz substrate. These nanowires have

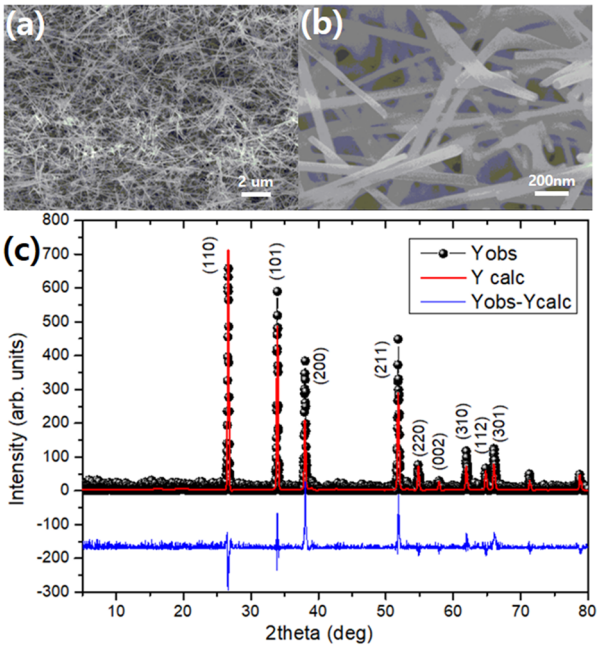

Figure 1. Morphological properties of SnO_2 nanowires. (a) SEM image of SnO_2 nanowires at a resolution of 10 μm. (b) Magnified SEM image of SnO_2 nanowires at a resolution of 1um. (c) Rietveld-refined XRD spectrum of the SnO_2 nanowires.

lengths of several micrometers and were grown randomly. Although most of the nanowires have smooth sidewalls, they are entangled with each other. Figure 1(c) shows the Rietveld refinement of the XRD data. Rietveld refinement was performed assuming a tetragonal structure ($P4_2/mnm$). The best matches between all the Miller indices and peaks of the experimental (Y_{obs}) and calculated (Y_{calc}) were obtained using the Rietveld parameters: R_p = 52.4, R_{wp} = 58.4, R_{exp} = 30.52, and χ^2 = 3.66. The atomic arrangement and crystalline parameters are listed in Table 1. SnO_2 has a rutile structure. The results confirm the presence of oxygen vacancies at a Sn/O ratio of 0.9:1.7 (1:1.889).

Table 1. Crystal Parameters and Atomic Positions of the SnO_2 Sample[a]

atom	Wyckoff position	valence	x	y	z	occupancy
Sn	A	+4	0	0	0	0.9
O	F	−2	0.32	0.32	0	1.7

[a]Crystal structure: tetragonal, space group: $P4_2/mnm$ (a = 4.735 Å; c = 3.185 Å).

The room-temperature Raman spectra of the SnO_2 nanowires in Figure 2 show peaks at 478, 635, and 776 cm^{-1}, in

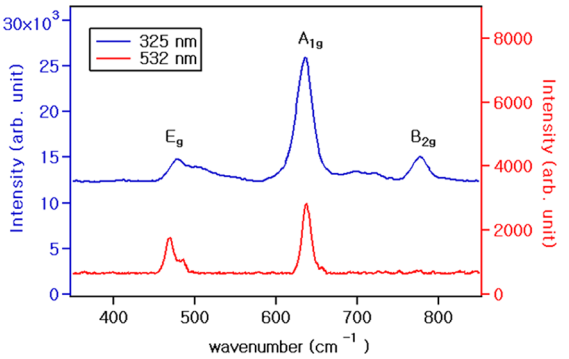

Figure 2. Raman spectra of SnO_2 nanowires. Raman shift peaks at 478, 635, and 776 cm^{-1} are attributed to the E_g, A_{1g}, and B_{2g} vibration modes of SnO_2, respectively.

good agreement with those of a single crystal of rutile SnO_2.[20] These peaks correspond to the E_g, A_{1g}, and B_{2g} vibration modes of SnO_2, respectively.[21,22] The nondegenerate A_{1g} and B_{2g} modes vibrate in the plane perpendicular to the c axis, while the E_g mode (doubly degenerate) vibrates in the direction of the c axis. Under excitation at 325 nm, all the modes are well-constructed, whereas the B_{2g} mode at 776 cm^{-1} does not appear under 532 nm excitation. Because UV light has a shorter penetration depth than visible light, the surface, dangling bonds on the surface and bonds perpendicular to the surface, is very sensitive to UV light. Thus, UV Raman spectroscopy is a valuable tool for investigating surface phenomena. The Raman spectra in Figure 2 indicate that the B_{2g} mode of the SnO_2 nanowires is more active on the surface than in the surface.

Figure 3(a) shows the PL spectra of SnO_2 nanowires between 13 and 310 K under excitation at 325 nm. There are two distinctive main peaks centered at 515 nm (2.4 eV) and 630 nm (1.96 eV). Each of these peaks displays several small peaks or bumps, and together they indicate color switching from green to orange at 100 K. There are three temperature regions that exhibit different PL behaviors. Below 70 K, green luminescence centered at 515 nm is dominant, and the green luminescence decreases dramatically with increasing temperature (Figure 3(b)). Above 100 K, the PL spectra exhibit orange luminescence centered at approximately 630 nm, which becomes more intense with increasing temperature up to 230

https://doi.org/10.1021/acs.jpcc.1c02937
J. Phys. Chem. C XXXX, XXX, XXX−XXX

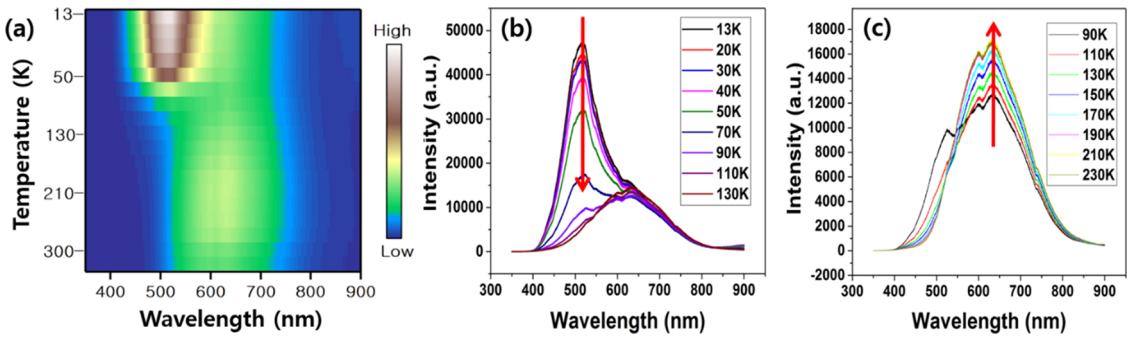

Figure 3. (a) PL spectra of SnO_2 nanowires at different temperatures. PL spectra in different temperature ranges: (b) below 130 K and (c) between 100 and 230 K. The main peaks correspond to different surface oxygen vacancy sites, and several minor peaks correspond to various shallow defect levels.

K (Figure 3(c)). (See Figures S1−S3 for deconvolution results of the PL spectra at different temperatures.)

According to previous experimental and computational results for the PL of SnO_2 nanowires,[21−27] the PL mechanisms are strongly related to surface defects such as oxygen vacancies. There are two types of oxygen sites at the surface (Scheme 1);

Scheme 1. Structure of SnO_2. Blue and Red Balls Denote Tin and Oxygen Atoms, Respectively

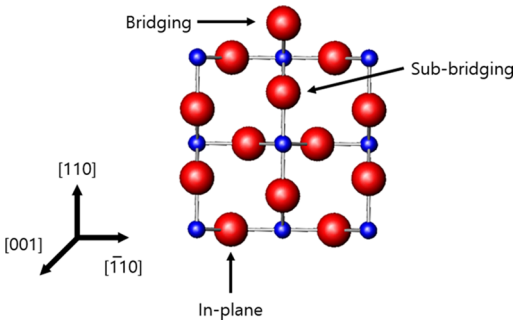

oxygen atoms aligned along the out-of-plane direction are called bridging oxygen (Ov_Bridge), and those in the in-plane direction of the nanowire are called in-plane oxygen (Ov_In-plane). Vacancies located at these two oxygen sites produce different defect levels (Scheme 2a,b).[28] The out-of-plane and in-plane oxygen vacancies correspond to orange (higher temperature) and green PL (lower temperature) via recombination from bulk oxygen vacancies (Ov_Bulk), where the states are located 0.3−0.15 eV below the conduction band minimum.[28−32]

Scheme 2. Schematic Drawing of the Color Switching Mechanism Depending on the Temperature and Position[a]

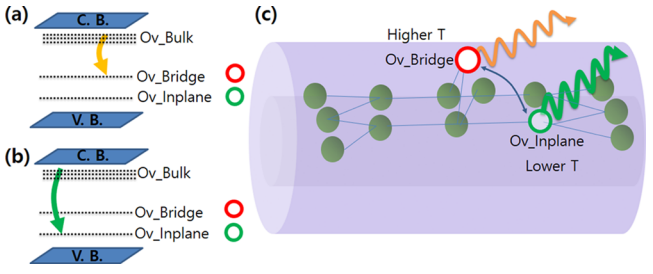

[a](a) Charge transfer from Ov_Bulk states to Ov_Bridge states: orange emission. (b) Charge transfer from Ov_Bulk states to Ov_Inplane states: green emission. (c) Oxygen vacancy migration with temperature. Oxygen vacancies occupy the bridge sites at room temperature, while they occupy the in-plane sites at low temperature.

On the basis of the origins of each PL color, we suggest that the change in color at 100 K is due to the redistribution of oxygen vacancies. The in-plane oxygen vacancies move to the bridging oxygen sites with increasing temperature. The large decrease in the green PL as the temperature increases up to 100 K indicates that the redistribution or migration of oxygen vacancies is accelerated.

Figure 4(a) shows a scanning transmission X-ray microscopy (STXM) image of SnO_2 nanowires with a spatial resolution of 30 nm. The radius of the wires is approximately 200 nm. Dark (bright) regions indicate more (less) absorption and less (more) transmission at the soft X-ray O K-edge. Because STXM is bulk-sensitive owing to the transmission geometry, the X-rays transmitted through the core produce a dark image, whereas those that passed only through shallow regions produce a bright image.

The oxygen *K*-edge XAS spectra in Figure 4(b,c) were collected in transmission mode from the regions marked by blue and pink lines in Figure 4(a). The two main peaks, denoted as A and B, are sharp and broad, respectively. Peaks A (Sn^{4+}, Sn^{3+}) and B (Sn^{+}, Sn^{2+}) are assigned to transitions of the O (1s) electrons to the hybridized orbitals of the O (2p) and Sn (5s) states and to the hybridized orbitals of the O (2p) and Sn (5p) states, respectively.[33,34] Sn has four valence electrons ($5s^2p^2$). Peak A is associated primarily with the bridging oxygen orbital, and in-plane oxygen vacancies uniformly distribute in the O *K*-edge spectra.[33] The charge transfer between peaks A and peaks B appears more distinct in fluorescence mode than in transmission mode (see Figure S4) When SnO_2 changes to SnO (an increase in oxygen vacancies), peak B increases, and peak A disappears.[34]

In Figure 4(b), the intensity of peak A obtained near the region of the center is higher than that from the surface. At 100 K, the intensity of peak A from the bulk decreases, while that of peak A from the surface increases. An important difference between the spectra obtained at 100 and 300 K appears in peaks A and B. The higher intensity of peak A at low temperature is probably associated with the decrease in bridging oxygen vacancies because at low temperature the orange PL decreases, whereas the increase in peak B indicates that the in-plane oxygen vacancies that are uniformly distributed at the O K-edge increase, suggesting that the movement of oxygen vacancies from bridging to in-plane sites at the surface of the wire with decreasing temperature is crucial

https://doi.org/10.1021/acs.jpcc.1c02937
J. Phys. Chem. C XXXX, XXX, XXX−XXX

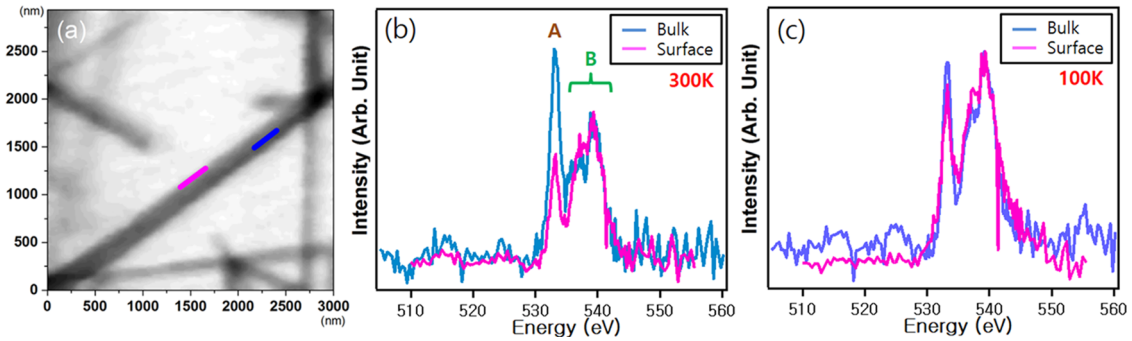

Figure 4. STXM image and X-ray absorption spectroscopy (XAS) spectra of SnO_2 nanowires at different temperatures. (a) STXM image of SnO_2 nanowires. (b) O *K*-edge XAS spectra at 300 K of blue and pink regions in (a). (c) O *K*-edge XAS spectra at 100 K of blue and pink regions in (a).

to the change in color after the temperature decrease (Scheme 2c). The removal or creation of oxygen vacancies is thought to be forbidden in this temperature range.[35] The similar shape of the spectra obtained at low temperature and room temperature also indicates that there is no significant removal or creation of oxygen vacancies in SnO_2.

4. CONCLUSIONS

The strong temperature dependence of PL in one-dimensional SnO_2 nanowires was investigated. Below 90 K, green emission is dominant, where orange luminescence appears above 90 K. The origin of the thermally induced color change is the migration of oxygen vacancies depending on the temperature and position. These results confirm the important role of oxygen vacancies in the performance of SnO_2 nanowires in optoelectronic devices, photocatalytic materials, and oxygen sensors. Furthermore, the results suggest that the luminescence color can be controlled via control of the distribution of oxygen vacancies in oxides by manipulation of the heat-treatment conditions such as cooling speed, oxygen pressure, and annealing temperature.

■ ASSOCIATED CONTENT

Supporting Information

The Supporting Information is available free of charge at https://pubs.acs.org/doi/10.1021/acs.jpcc.1c02937.

Photoluminescence spectra of SnO2 nanowires at different temperatures were deconvoluted using Gaussian curves; fitting parameters such as location, full width at half maximum (FWHM), amplitude, and area (Table S1, Table S2, and Table S3); and oxygen *K*-edge spectra in SnO_2 taken at 30 K (red) and 300 K (blue) in fluorescence mode (Figure S4) (PDF)

■ AUTHOR INFORMATION

Corresponding Authors

Dongwook Lee − *Department of Physics, College of Science and Technology, Yonsei University, Wonju-si, Gangwon-do 26493, Republic of Korea; LnR Tech Co. Ltd., 2235-12 Wonju-si, Gangwondo, Republic of Korea;* orcid.org/0000-0002-0787-8305; Email: dongwookleedl324@lnr-tech.com, dongwookleedl324@gmail.com

Jiwon Seo − *Department of Physics, College of Science and Technology, Yonsei University, Wonju-si, Gangwon-do 26493, Republic of Korea*; Email: jiwonseo@yonsei.ac.kr

Authors

Euiyoung Choi − *Department of Physics, College of Science and Technology, Yonsei University, Wonju-si, Gangwon-do 26493, Republic of Korea*

Hyun-Joon Shin − *Department of Physics, Chungbuk National University, Cheongju, Chungbuk 28644, Republic of Korea*

Namdong Kim − *Pohang Accelerator Laboratory, Pohang 37673, Republic of Korea*

L. De Los Santos Valladares − *Cavendish Laboratory, Department of Physics, University of Cambridge, Cambridge CB3 0HE, United Kingdom; School of Materials Science and Engineering, Northeastern University, Shenyang 110819, People's Republic of China; Laboratorio de Cerámicos y Nanomateriales, Facultad de Ciencias Física, Universidad Nacional Mayor de San Marcos, 14-0149 Lima, Perú*

Complete contact information is available at: https://pubs.acs.org/10.1021/acs.jpcc.1c02937

Notes

The authors declare no competing financial interest.

■ ACKNOWLEDGMENTS

This work was supported by the National Research Foundation of President Post-doctoral fellowship Program (NRF-2013R1A6A3A060443). L. De Los Santos Valladares thanks the Incorporación de Investigadores Program from the CONCYTEC − World Bank - UNMSM (Contrat No. 12 -2019 − FONDECYT − BM − INC. INV.) for supporting his research at the University of San Marcos, Peru.

■ REFERENCES

(1) Godinho, K. G.; Walsh, A.; Watson, G. W. Energetic and Electronic Structure Analysis of Intrinsic Defects in Sno2. *J. Phys. Chem. C* **2009**, *113*, 439−448.

(2) Chopra, K. L.; Major, S.; Pandya, D. K. Transparent Conductors—a Status Review. *Thin Solid Films* **1983**, *102*, 1−46.

(3) Stjerna, B.; Granqvist, C. G.; Seidel, A.; Häggström, L. Characterization of Rf-Sputtered Snox Thin Films by Electron Microscopy, Hall-Effect Measurement, and Mössbauer Spectrometry. *J. Appl. Phys.* **1990**, *68*, 6241−6245.

(4) Kılıç, Ç.; Zunger, A. Origins of Coexistence of Conductivity and Transparency in Sno2. *Phys. Rev. Lett.* **2002**, *88*, No. 095501.

(5) Kim, H.; Auyeung, R. C. Y.; Piqué, A. Transparent Conducting F-Doped Sno2 Thin Films Grown by Pulsed Laser Deposition. *Thin Solid Films* **2008**, *516*, 5052−5056.

(6) Okuya, M.; Kaneko, S.; Hiroshima, K.; Yagi, I.; Murakami, K. Low Temperature Deposition of Sno2 Thin Films as Transparent

Electrodes by Spray Pyrolysis of Tetra-N-Butyltin(Iv). *J. Eur. Ceram. Soc.* **2001**, *21*, 2099−2102.
(7) Das, S.; Jayaraman, V. Sno2: A Comprehensive Review on Structures and Gas Sensors. *Prog. Mater. Sci.* **2014**, *66*, 112−255.
(8) Yang, D.-J.; Kamienchick, I.; Youn, D. Y.; Rothschild, A.; Kim, I.-D. Ultrasensitive and Highly Selective Gas Sensors Based on Electrospun Sno2 Nanofibers Modified by Pd Loading. *Adv. Funct. Mater.* **2010**, *20*, 4258−4264.
(9) Song, Z.; Wei, Z.; Wang, B.; Luo, Z.; Xu, S.; Zhang, W.; Yu, H.; Li, M.; Huang, Z.; Zang, J.; et al. Sensitive Room-Temperature H2s Gas Sensors Employing Sno2 Quantum Wire/Reduced Graphene Oxide Nanocomposites. *Chem. Mater.* **2016**, *28*, 1205−1212.
(10) Snaith, H. J.; Ducati, C. Sno2-Based Dye-Sensitized Hybrid Solar Cells Exhibiting near Unity Absorbed Photon-to-Electron Conversion Efficiency. *Nano Lett.* **2010**, *10*, 1259−1265.
(11) Ren, X.; Yang, D.; Yang, Z.; Feng, J.; Zhu, X.; Niu, J.; Liu, Y.; Zhao, W.; Liu, S. F. Solution-Processed Nb:Sno2 Electron Transport Layer for Efficient Planar Perovskite Solar Cells. *ACS Appl. Mater. Interfaces* **2017**, *9*, 2421−2429.
(12) Tiwana, P.; Docampo, P.; Johnston, M. B.; Snaith, H. J.; Herz, L. M. Electron Mobility and Injection Dynamics in Mesoporous Zno, Sno2, and Tio2 Films Used in Dye-Sensitized Solar Cells. *ACS Nano* **2011**, *5*, 5158−5166.
(13) Liu, L.-C.; Chen, J.-S.; Jeng, J.-S. Role of Oxygen Vacancies on the Bias Illumination Stress Stability of Solution-Processed Zinc Tin Oxide Thin Film Transistors. *Appl. Phys. Lett.* **2014**, *105*, No. 023509.
(14) Yang, S.; Ji, K. H.; Kim, U. K.; Hwang, C. S.; Park, S.-H. K.; Hwang, C.-S.; Jang, J.; Jeong, J. K. Suppression in the Negative Bias Illumination Instability of Zn-Sn-O Transistor Using Oxygen Plasma Treatment. *Appl. Phys. Lett.* **2011**, *99*, 102103.
(15) Zhang, F.; Ma, W.; Guo, H.; Zhao, Y.; Shan, X.; Jin, K.; Tian, H.; Zhao, Q.; Yu, D.; Lu, X.; et al. Interfacial Oxygen Vacancies as a Potential Cause of Hysteresis in Perovskite Solar Cells. *Chem. Mater.* **2016**, *28*, 802−812.
(16) Zhong, Y.; Li, W.; Zhao, X.; Jiang, X.; Lin, S.; Zhen, Z.; Chen, W.; Xie, D.; Zhu, H. High-Response Room-Temperature No2 Sensor and Ultrafast Humidity Sensor Based on Sno2 with Rich Oxygen Vacancy. *ACS Appl. Mater. Interfaces* **2019**, *11*, 13441−13449.
(17) Xu, Y.; Zheng, L.; Yang, C.; Zheng, W.; Liu, X.; Zhang, J. Oxygen Vacancies Enabled Porous Sno2 Thin Films for Highly Sensitive Detection of Triethylamine at Room Temperature. *ACS Appl. Mater. Interfaces* **2020**, *12*, 20704−20713.
(18) Sohal, M. K.; Mahajan, A.; Gasso, S.; Nahirniak, S. V.; Dontsova, T. A.; Singh, R. C. Modification of Sno2 Surface Oxygen Vacancies through Er Doping for Ultralow No2 Detection. *Mater. Res. Bull.* **2021**, *133*, No. 111051.
(19) Du, W.; Si, W.; Wang, F.; Lv, L.; Wu, L.; Wang, Z.; Liu, J.; Liu, W. Creating Oxygen Vacancies on Porous Indium Oxide Nano-spheres Via Metallic Aluminum Reduction for Enhanced Nitrogen Dioxide Detection at Low Temperature. *Sens. Actuators B* **2020**, *303*, No. 127221.
(20) Scott, J. F. Raman Spectrum of Sno2. *J. Chem. Phys.* **1970**, *53*, 852−853.
(21) Yu, K. N.; Xiong, Y.; Liu, Y.; Xiong, C. Microstructural Change of Nano-Sno2 Grain Assemblages with the Annealing Temperature. *Phys. Rev. B* **1997**, *55*, 2666−2671.
(22) Peercy, P. S.; Morosin, B. Pressure and Temperature Dependences of the Raman-Active Phonons in Sno2. *Phys. Rev. B* **1973**, *7*, 2779−2786.
(23) Cabot, A.; Arbiol, J.; Ferré, R.; Morante, J. R.; Chen, F.; Liu, M. Surface States in Template Synthesized Tin Oxide Nanoparticles. *J. Appl. Phys.* **2004**, *95*, 2178−2180.
(24) Sundaram, K. B.; Bhagavat, G. K. Optical Absorption Studies on Tin Oxide Films. *J. Phys. D Appl. Phys.* **1981**, *14*, 921−925.
(25) Takagahara, T.; Hanamura, E. Giant-Oscillator-Strength Effect on Excitonic Optical Nonlinearities Due to Localization. *Phys. Rev. Lett.* **1986**, *56*, 2533−2536.
(26) Kayanuma, Y. Quantum-Size Effects of Interacting Electrons and Holes in Semiconductor Microcrystals with Spherical Shape. *Phys. Rev. B* **1988**, *38*, 9797−9805.
(27) Luo, S.; Fan, J.; Liu, W.; Zhang, M.; Song, Z.; Lin, C.; Wu, X.; Chu, P. K. Synthesis and Low-Temperature Photoluminescence Properties of Sno2nanowires and Nanobelts. *Nanotechnology* **2006**, *17*, 1695−1699.
(28) Prades, J. D.; Arbiol, J.; Cirera, A.; Morante, J. R.; Avella, M.; Zanotti, L.; Comini, E.; Faglia, G.; Sberveglieri, G. Defect Study of Sno2 Nanostructures by Cathodoluminescence Analysis: Application to Nanowires. *Sens. Actuators B* **2007**, *126*, 6−12.
(29) Kim, T. W.; Lee, D. U.; Yoon, Y. S. Microstructural, Electrical, and Optical Properties of Sno2 Nanocrystalline Thin Films Grown on Inp (100) Substrates for Applications as Gas Sensor Devices. *J. Appl. Phys.* **2000**, *88*, 3759−3761.
(30) Kim, H. W.; Kim, N. H.; Myung, J. H.; Shim, S. H. Characteristics of Sno2 Fishbone-Like Nanostructures Prepared by the Thermal Evaporation. *Phys. Status Solidi A* **2005**, *202*, 1758−1762.
(31) Ma, J.; Wang, Y.; Ji, F.; Yu, X.; Ma, H. Uv−Violet Photoluminescence Emitted from Sno2:Sb Thin Films at Different Temperature. *Mater. Lett.* **2005**, *59*, 2142−2145.
(32) Gu, F.; Fen Wang, S.; Feng Song, C.; Kai Lü, M.; Xin Qi, Y.; Jun Zhou, G.; Xu, D.; Rong Yuan, D. Synthesis and Luminescence Properties of Sno2 Nanoparticles. *Chem. Phys. Lett.* **2003**, *372*, 451−454.
(33) Moreno, M. S.; Egerton, R. F.; Rehr, J. J.; Midgley, P. A. Electronic Structure of Tin Oxides by Electron Energy Loss Spectroscopy and Real-Space Multiple Scattering Calculations. *Phys. Rev. B* **2005**, *71*, No. 035103.
(34) Chang, G. S.; Forrest, J.; Kurmaev, E. Z.; Morozovska, A. N.; Glinchuk, M. D.; McLeod, J. A.; Moewes, A.; Surkova, T. P.; Hong, N. H. Oxygen-Vacancy-Induced Ferromagnetism in Undoped Sno2 Thin Films. *Phys. Rev. B* **2012**, *85*, No. 165319.
(35) Cox, D. F.; Fryberger, T. B.; Semancik, S. Oxygen Vacancies and Defect Electronic States on the Sno2(110)-1x1 Surface. *Phys. Rev. B* **1988**, *38*, 2072−2083.

https://doi.org/10.1021/acs.jpcc.1c02937
J. Phys. Chem. C XXXX, XXX, XXX−XXX